Electronic coupling calculation and pathway analysis of electron transfer reaction using ab initio fragment-based method. I. FMO–LCMO approach

Hirotaka Nishioka and Koji Ando

Citation: The Journal of Chemical Physics **134**, 204109 (2011); doi: 10.1063/1.3594100
View online: http://dx.doi.org/10.1063/1.3594100
View Table of Contents: http://scitation.aip.org/content/aip/journal/jcp/134/20?ver=pdfcov
Published by the AIP Publishing

Electronic coupling calculation and pathway analysis of electron transfer reaction using *ab initio* fragment-based method. I. FMO–LCMO approach

Hirotaka Nishioka[a] and Koji Ando
Department of Chemistry, Graduate School of Science, Kyoto University, Sakyo-ku, Kyoto 606-8502, Japan

(Received 9 March 2011; accepted 5 May 2011; published online 26 May 2011)

By making use of an *ab initio* fragment-based electronic structure method, fragment molecular orbital–linear combination of MOs of the fragments (FMO–LCMO), developed by Tsuneyuki *et al.* [Chem. Phys. Lett. **476**, 104 (2009)], we propose a novel approach to describe long-distance electron transfer (ET) in large system. The FMO–LCMO method produces one-electron Hamiltonian of whole system using the output of the FMO calculation with computational cost much lower than conventional all-electron calculations. Diagonalizing the FMO–LCMO Hamiltonian matrix, the molecular orbitals (MOs) of the whole system can be described by the LCMOs. In our approach, electronic coupling T_{DA} of ET is calculated from the energy splitting of the frontier MOs of whole system or perturbation method in terms of the FMO–LCMO Hamiltonian matrix. Moreover, taking into account only the valence MOs of the fragments, we can considerably reduce computational cost to evaluate T_{DA}. Our approach was tested on four different kinds of model ET systems with non-covalent stacks of methane, non-covalent stacks of benzene, trans-alkanes, and alanine polypeptides as their bridge molecules, respectively. As a result, it reproduced reasonable T_{DA} for all cases compared to the reference all-electron calculations. Furthermore, the tunneling pathway at fragment-based resolution was obtained from the tunneling current method with the FMO–LCMO Hamiltonian matrix.
 [doi:10.1063/1.3594100]

I. INTRODUCTION

Electron transfer (ET) reactions play important roles in biological functions such as photosynthesis, respiration, and DNA repair. In these biological systems, the superexchange mechanism significantly works;[1,2] the ET takes place via the long-distance electron tunneling between redox centers separated by more than several angstroms (Å) where the tunneling electron uses the electronic states of the protein environment as its virtual intermediate states. The superexchange mechanism dominantly contributes to the electronic coupling T_{DA} in the following non-adiabatic formula:[3,4]

$$k_{DA} = \frac{2\pi}{\hbar}|T_{DA}|^2(\mathrm{FC}), \tag{1}$$

where (FC) is the thermally averaged Franck-Condon factor. Therefore, the ET rate remarkably depends on the nature of the intervening protein media via T_{DA}.[5]

For these decades, qualitative estimation of T_{DA} from structural information of bridge has been recognized to be an important subject to understand long-distance ETs at molecular level. Several theoretical techniques to calculate T_{DA} and to analyze the tunneling pathway have been developed (for reviews, see Refs. 6–9). Many studies of biological ETs have been conducted using the *Pathways* model,[10–12] packing density model,[13,14] and semiempirical quantum chemical (QM) methods, such as extended-Hückel,[12,15–22] and neglect of differential overlap methods.[23–29] More accurate estimation of T_{DA} requires *ab initio* QM methods, whose applications, however, have been limited to rather small donor-acceptor complexes linked by organic spacer molecules.[6,30–37] The reason for the scarceness of *ab initio* QM studies on biological ET systems is not simply because of their huge computational cost, but also of the need to consider thermal fluctuation of protein conformation that causes large variations in T_{DA}. This aspect has been revealed by combined studies with molecular dynamics (MD) simulations;[38–46] from the non-Condon theories for ET,[39,47–51] the qualitative estimation of the ET rate should need the statistical average of $|T_{DA}|^2$ taken over sufficiently many configurations from MD simulations (for reviews, see Refs. 52 and 53). To our knowledge, a few combined studies[54–58] of *ab initio* QM methods with MD simulations have been conducted for fluctuating protein structures, as well as studies with *ab initio* QM methods for fixed protein structures.[59–63]

Under this situation, the QM methods with specific algorithms aimed at large systems[64–66] have potential to overcome the difficulty in application of *ab initio* QM methods to biological ET systems. Among them, the fragment-based QM methods that have been developed actively and applied to various large systems[67–79] will be advantageous. In the *ab initio* fragment-based methods, such as fragment molecular orbital (FMO) method[66,69–71] and divide-and-conquer (DC) method,[75–79] the total system is first divided into small fragments. Electronic calculation on each fragment is then performed and the properties of the total system, such as the total energy, are calculated from the results of the fragments. The fragment-based methods can reduce the total computational time, do not require preparation of the initial MOs or the electronic density of the total system for the

[a]Author to whom correspondence should be addressed. Electronic mail: nishioka@kuchem.kyoto-u.ac.jp.

self-consistent field (SCF) procedure, and fit well with the parallel-computing technology.

In the area of ET, Kurinikov and Beratan[62] have developed an *ab initio* fragment-based method for calculating T_{DA} of large molecules. In their method, the effective Hamiltonian in the space of valence atomic orbitals for each isolated fragment is first calculated by using the Löwdin's partitioning[80,81] or closely related projection operator[82] techniques, from which the effective Hamiltonian of the total system is constructed. Their method has been applied to several ET systems.[63,83,84]

As a related but potentially more efficient and versatile alternative, we propose in this paper a novel approach to calculate T_{DA} and analyze the tunneling pathway of long-distance ET by making use of the FMO–LCMO (linear combination of molecular orbitals) method developed recently by Tsuneyuki *et al.*[85] In contrast to the original FMO,[69–71] the FMO–LCMO method can produce the total Hamiltonian matrix and molecular orbitals (MOs) of whole system from the fragment monomer and dimer outputs of FMO calculations.[85] Exploiting this method, we calculate the T_{DA} values from the MO energy splitting or by a perturbation method. Moreover, we have obtained the tunneling pathways at fragment-based resolution by combining the tunneling current methods[9,18,19] with the FMO–LCMO Hamiltonian matrix. Our approach was tested on four different kinds of model ET systems and produced reasonable results in comparison with the conventional *ab initio* QM approach. (Throughout this paper, "conventional" means the all-electron calculation of the entire non-fragmented system.) In particular, we have found that the size reduction of the FMO–LCMO method to the valence-only space is quite straightforward, accurate, and thus useful to calculate T_{DA} for large ET systems.

II. THEORY

A. FMO–LCMO

Here we briefly review the FMO–LCMO method, whose details have been described in Ref. 85.

The FMO–LCMO calculation is based on the result of FMO calculation with fragment dimer correction (FMO2). In the FMO2 method,[69,70] the total molecule is first divided into N fragments. The electronic structure of each fragment monomer is solved self-consistently in the Coulomb field of all other fragment monomers, and then the electronic structure of each fragment dimer is solved in the Coulomb field of all other fragments.[69,70] The FMO2 method approximates the total electronic energy of the system, E_{total}, as follows:

$$E_{\text{total}} = \sum_{I>J} E_{IJ} - (N-2)\sum_{I} E_I, \tag{2}$$

where E_I and E_{IJ} are the electronic energies of the fragment monomer I and the fragment dimer IJ, respectively. We express the pth canonical MO and corresponding orbital energy for the fragment monomer I as $|\phi_p^I\rangle$ and ϵ_{I_p}, respectively. Similarly, the ath canonical MO and corresponding orbital energy for the fragment dimer IJ are expressed as $|\phi_a^{IJ}\rangle$ and ϵ_{IJ_a}.

Using these canonical MOs and the orbital energies, one-electron Hamiltonian matrices of fragment monomers and dimers can be written as

$$(H_I)_{I_p,I_q} = \epsilon_{I_p}\delta_{I_p,I_q}, \tag{3}$$

$$(H_{IJ})_{IJ_a,IJ_b} = \epsilon_{IJ_a}\delta_{IJ_a,IJ_b}. \tag{4}$$

When bond-detached atoms (BDAs) (Refs. 70 and 71) exist, one should remove from Eqs. (3) and (4) the monomer and dimer MOs with anomalous eigenvalues produced by the projection operators.[85] (Details are described in the next paragraph.) One-electron Hamiltonian matrix of fragment dimers in the dimer MO representation can be transformed into monomer MO representation as follows:

$$(H_{IJ})_{L_p,M_q} = \sum_{IJ_a} \epsilon_{IJ_a}\langle\phi_p^L|\phi_a^{IJ}\rangle\langle\phi_a^{IJ}|\phi_q^M\rangle. \tag{5}$$

The FMO–LCMO method assumes the following forms for the total one-electron Hamiltonian matrix in the monomer MO representation:

$$(H_{\text{total}})_{Ip,Jq} = (H_{IJ})_{Ip,Jq} \quad \text{for } I \neq J, \tag{6}$$

$$(H_{\text{total}})_{Ip,Iq} = \sum_{J\neq I}(H_{IJ})_{Ip,Iq} - (N-2)(H_I)_{Ip,Iq}. \tag{7}$$

Here, the diagonal blocks, Eq. (7), have the same form as Eq. (2). The MOs and corresponding energies for the total system can be obtained by solving a generalized eigenvalues problem of the total Hamiltonian matrix with overlap matrix of monomer MOs.

We now comment about the BDA. When covalent bonds are cut for dividing a system into fragments in the FMO calculations, the FMO–LCMO method needs the following treatments.[85] The FMO method uses the projection operators to divide the basis functions on the BDAs (junction atoms) along the natural localized molecular orbitals (NLMOs) and to preserve these bond electron pairs.[70,71] When the single bond between carbon atoms ($C_\alpha - C$ bonds for protein) are cut, the projection operator divides the $1s$ and four sp^3 orbitals on the BDA (C_α for protein) 4:1, where 4 (one s NLMO and three of four sp^3 NLMOs) belong to one fragment and 1 (the remaining sp^3 NLMO) belongs to the other fragment. Due to the use of shift operator with high energy parameter in the projection, these treatments produce monomer and dimer MOs with anomalous eigenvalues. In the FMO–LCMO method, these anomalous MOs should be removed when the one-electron Hamiltonians $(H_I)_{I_p,I_q}$ and $(H_{IJ})_{IJ_a,IJ_b}$ in Eqs. (3) and (4) are constructed.[85] However, with the basis sets larger than the minimal ones, this purification involves overcompleteness in the basis sets, thereby causing problem in the diagonalization of the FMO–LCMO Hamiltonian matrix.[85] In this study, we shall not pursue this technical problem but just employ the minimal basis sets when BDAs are involved.

In the FMO–LCMO method, limiting the number of monomer MOs expanding the matrices Eqs. (3) and (5) can reduce the size of the total Hamiltonian matrix Eqs. (6) and (7).[85] This matrix-size reduction can considerably reduce computational cost for both constructing and diagonalizing

the total Hamiltonian matrix. To remove arbitrariness in the selection of monomer MOs, in this work we exclusively consider reduction to the valence MOs. We call this the FMO with linear combination of valence molecular orbitals (FMO–LCVMO), which will also be examined for calculation of T_{DA} and analysis of the tunneling pathway.

B. Electronic coupling, perturbation method, and bridge Green's function matrix

In the two-state approximation, the T_{DA} can be obtained from the half energy difference between the two quasi-degenerate adiabatic states $|\psi^+\rangle$ and $|\psi^-\rangle$ at the transition state conformation:[6]

$$|T_{DA}| = \frac{|\epsilon_- - \epsilon_+|}{2}, \tag{8}$$

where ϵ_+ and ϵ_- are the energies of $|\psi^+\rangle$ and $|\psi^-\rangle$, respectively. For the biological ET systems, the Hartree-Fock (HF) Koopmans' theorem (KT) scheme[6,9,30,31] is useful and normally sufficient to approximate the T_{DA}-value.[54–56,58] In the HF-KT scheme, the ϵ_+ and ϵ_- in Eq. (8) are assumed to be the energies of the two HF MOs mostly contributing to the electron tunneling. (In most cases, such two MOs correspond to the two highest-lying occupied MOs (HOMOs) or the two lowest-lying unoccupied MOs (LUMOs).) In this study, we used the one-electron picture based on the HF-KT scheme and obtained (and compared) the MOs from the conventional HF and the FMO–LC(V)MO calculations. The orbital energies and the wave functions we adopted are described in Sec. III B.

If the two specific monomer MOs are adopted as the donor and acceptor orbitals, ϕ_D and ϕ_A, the electronic coupling can be approximated by the following perturbation method:[6–9,24,35,62,86]

$$T_{DA} = \sum_{I,J}^{N} \sum_{I_p, J_q(\neq \phi_D, \phi_A)} \left(E_{\rm tun} S_{\phi_D, I_p} - H_{\phi_D, I_p}\right) \times G^B(E_{\rm tun})_{I_p, J_q} \left(E_{\rm tun} S_{J_q, \phi_A} - H_{J_q, \phi_A}\right), \tag{9}$$

where the H represents one-electron FMO–LCMO Hamiltonian matrix in Eqs. (6) and (7) and the S represents overlap matrix of nonorthogonal monomer MOs. The matrix $\mathbf{G}^B(E_{\rm tun})$ is the bridge Green function matrix as,

$$\mathbf{G}^B(E_{\rm tun}) = [E_{\rm tun} S^B - H^B]^{-1}. \tag{10}$$

in which $E_{\rm tun}$ is the tunneling energy parameter. In this study, $E_{\rm tun}$ is set to the average value between the donor and acceptor MO energies.

C. Inter-fragment tunneling currents

In this study, we used one-electron formulation of tunneling currents[9,18,19] for the pathway analysis. Here we briefly show the theoretical formula of the tunneling current among fragment monomer orbitals and their application to the calculation of T_{DA}.

We first express the molecular orbitals $|\psi^i\rangle$ and $|\psi^f\rangle$ in the initial and final diabatic states in terms of fragment monomer orbitals $|\phi_{I_p}\rangle$ as follows:

$$|\psi^i\rangle = C_D^i |\phi_D\rangle + \sum_{I}^{N} \sum_{I_p} C_{I_p}^i |\phi_{I_p}\rangle, \tag{11}$$

$$|\psi^f\rangle = C_A^f |\phi_A\rangle + \sum_{I}^{N} \sum_{I_p} C_{I_p}^f |\phi_{I_p}\rangle, \tag{12}$$

where ϕ_D and ϕ_A are the donor and acceptor orbitals, respectively, which are used in Eq. (9).

The tunneling current J_{L_p, M_q} between the monomer MOs ϕ_{L_p} and ϕ_{M_q} is then given by[9,18,19]

$$J_{L_p, M_q} = \frac{1}{\hbar}(H_{L_p, M_q} - E_{\rm tun} S_{L_p, L_q})\left(C_{L_p}^i C_{M_q}^f - C_{L_p}^f C_{M_q}^i\right). \tag{13}$$

Therefore, the tunneling current between fragments L and M is given by

$$J_{L,M} = \sum_{L_p} \sum_{M_q} J_{L_p, M_q}. \tag{14}$$

The electronic coupling calculated from the perturbative method in Eq. (9) is rewritten by using the tunneling currents as follows:[9,18,19]

$$T_{DA} = \hbar \sum_{L \in \Omega_D, M \notin \Omega_D} J_{L,M}, \tag{15}$$

where Ω_D is a donor side space separated from acceptor side.

The main pathways at fragment-based resolution can be visualized with the connecting vectors of the following normalized tunneling currents:[21,22,42–44]

$$K_{L,M} = \frac{\hbar(J_{L,M})}{T_{DA}}. \tag{16}$$

III. COMPUTATIONAL DETAILS

We have applied our approach to the four model ET systems shown in Fig. 1. These model systems have been used in the previous calculations of T_{DA} and Green function matrix with *ab initio* QM methods.[30,34,35,62] We shall emphasize that our approach is not restricted to the symmetric systems as in Figs. 1(a)–1(c). The choice is, as in the previous works, mainly because of the convenience in setting appropriate structures corresponding to the transition state.

Figure 1(a) illustrates the model system CH_3-$(CH_4)_3$-CH_3 where CH_3 molecules are donor/acceptor groups and non-covalent stacks of methane, $(CH_4)_3$, are bridge groups.[30] This system represents long-distance σ-type ET where the excess electron is exchanged between the lone pair orbitals of the two CH_3 molecules through non-covalent and saturated bridge groups.

Figure 1(b) illustrates the model system TCNE-$(C_6H_6)_n$-TCNE where tetracyanoethylene (TCNE) molecules are donor/acceptor groups and the non-covalent stacks of benzene, $(C_6H_6)_n$ $(n = 1, \ldots, 8)$, are bridge groups.[34] This system represents long-distance ET where the excess electron is exchanged between the π^* orbitals of the two TCNEs through non-covalent and unsaturated bridge groups.

Figure 1(c) illustrates the model system Be-C_nH_{2n+2}-Be, where Be atoms are donor/acceptor groups and trans n-alkanes, $C_nH_{2n+2}(n = 2, 4, \ldots, 18)$, are bridge groups.[35,62]

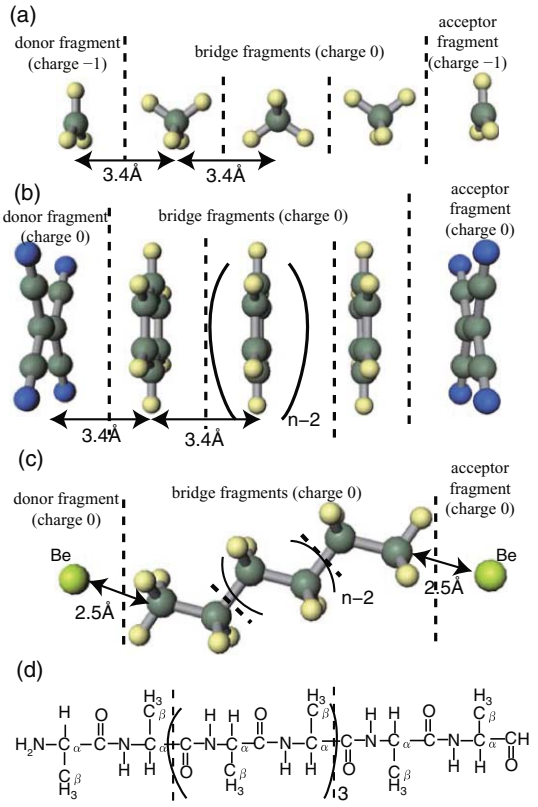

FIG. 1. Molecules used as model ET systems. (a) CH_3-$(CH_4)_3$-CH_3, (b) TCNE-$(C_6H_6)_n$-TCNE, (c) Be-C_nH_{2n+2}-Be systems, and (d) ala_{10}.

For this system, we investigate long-distance hole transfer where the excess hole is exchanged between the 2*s* orbitals of the two Be atoms through covalent and saturated bridge groups.

Figure 1(d) illustrates the model system ala_{10} where alanine polypeptides in α-helix and β-strand conformations are adopted as the isolated bridge groups.[62] For this system, we have investigated the isolated bridge Green's function matrix.

A. Structures

For the model ET systems in Figs. 1(a)–1(c), the transition state conformations are well defined by symmetry. In determining the structures of these systems, we basically followed the previous works[30,34,35,62] but with different basis set.

The structure of CH_3-$(CH_4)_3$-CH_3 was obtained as follows:[30] First, the coordinate of CH_4 molecule was determined by geometrical optimization with restricted Hartree-Fock (RHF)/6-311G(d,p), constrained to T_d symmetry; the coordinate of CH_3 molecule was determined for the anion singlet state by geometrical optimization with RHF/6-311G(d,p), constrained to C_{3v} symmetry; we then stacked the CH_3 and CH_4 molecules with the C-C distances of 3.4 Å so that the overall structure had C_{2v} symmetry (see Fig. 1(a)).

The structures of TCNE-$(C_6H_6)_n$-TCNE were obtained as follows:[34] First, the coordinate of benzene molecule was determined by geometrical optimization with RHF/6-311G(d,p) constrained to D_{6h} symmetry. The coordinate of TCNE molecule was determined similarly under D_{2h} symmetry. The TCNE and benzene molecules were then stacked with the intermolecular separation of 3.4 Å between the molecular planes so that the overall structure had D_{2h} symmetry as shown in Fig. 1(b).

The structures of Be-C_nH_{2n+2}-Be were obtained as follows:[35,62] First, the coordinate of C_nH_{2n+2} molecule was determined by geometrical optimization with RHF/6-311G(d,p), constrained to C_{2h} symmetry. Each Be atom was separated by 2.5 Å from the terminal carbon atom of C_nH_{2n+2} molecules so that the overall structure had C_{2h} symmetry as shown in Fig. 1(c).

The structures of ala_{10} were set to "idealized" α-helix and β-strand geometries.[62,87]

B. Electronic structure calculations

At the geometries obtained in Sec. II A, we performed both conventional RHF and FMO calculations. The charge and spin states are dianion singlet for CH_3-$(CH_4)_3$-CH_3 and neutral singlet for the other systems: TCNE-$(C_6H_6)_n$-TCNE, Be-C_nH_{2n+2}-Be, and ala_{10} in α-helix and β-strand conformations.

For calculating the anion couplings of CH_3-$(CH_4)_3$-CH_3 with the HF-KT scheme, we used the obtained HOMO-1 and HOMO orbitals as ψ^+ and ψ^- that are mostly symmetric and antisymmetric combinations of the lone pair orbitals of CH_3 molecules, respectively. For FMO calculation, the system was divided into the manner as shown by the vertical dashed lines in Fig. 1(a) where the terminal CH_3 was the donor or acceptor fragment and the remaining each CH_4 was treated as a bridge fragment. Total charges for donor/acceptor and bridge fragments were set to −1 and 0, respectively, as shown in Fig. 1(a).

For calculating the anion couplings of TCNE-$(C_6H_6)_n$-TCNE with the HF-KT scheme, we used the LUMO and LUMO+1 orbitals as ψ^+ and ψ^- that are mostly symmetric and antisymmetric combinations of the π^* orbitals of the TCNE molecules, respectively. For FMO calculation, the system was divided into the manner as shown by the vertical dashed lines in Fig. 1(a) where the terminal TCNE was the donor or acceptor fragment and the remaining each C_6H_6 was treated as a bridge fragment. Total charge for each fragment was set to 0 as shown in Fig. 1(a).

For calculating the cation couplings of Be-C_nH_{2n+2}-Be with the HF-KT scheme, we used the HOMO-1 and HOMO orbitals as ψ^+ and ψ^- that are mostly symmetric and antisymmetric combinations of the 2*s* atomic orbitals of the Be atoms, respectively. For FMO calculation, the system was divided into the manner as shown by the dashed lines in Fig. 1(c) where the Be atom was the donor or acceptor fragment and the remaining fragments were bridge ones. We divided the NLMOs on BDAs in the following two ways: (1) four of the five NLMOs on the BDA belong to the left fragment and the other one to the right fragment (see Fig. 1(c)). We call this BDA1. (2) We first divide the system into halves, then the left half follows the same way as BDA1, whereas for the right half the assignment was reversed so that the C_{2h} symmetry is preserved. We call this BDA2. The BDA2 was used for Be-C_nH_{2n+2}-Be ($n = 6$, 10, 14, and 18). Total charge for each fragment was set to 0 as shown in Fig. 1(c).

For FMO calculation of ala_{10}, the system was divided into the manner as shown by the vertical dashed lines in Fig. 1(d) where C_α's are bond-detached atoms and two residues were used per bridge fragment. Total charge for each fragment was set to 0.

In this study, we have used the FMO code[71] (version 3.2) implemented in the GAMESS program.[88] All FMO2 calculations involved no cutoff for approximating the SCF energy by electrostatic interaction. In all FMO2 calculations, all pairs of monomers were taken into account for dimer calculations. All the other electronic structure calculations, including geometrical optimization, were also performed using the GAMESS program.[88]

IV. RESULTS

A. CH_3-$(CH_4)_3$-CH_3 system

To obtain the FMO–LCMO total Hamiltonian used for the T_{DA} calculation and the pathway analysis, we first performed FMO2 calculations for the CH_3-$(CH_4)_3$-CH_3 system. To confirm their reliability, we also performed conventional HF calculations for the reference. In these calculations, we used several basis sets including the minimal basis set STO-3G, Pople basis sets[89–91] 3-21G, 6-31G(d), 6-311G, 6-311G(d), Dunning "correlation-consistent" basis sets cc-pVDZ and cc-pVTZ,[92] and the diffuse-function basis sets 3-21+G and 6-31++G(d,p).[93]

The total energies calculated from the conventional HF and FMO2 calculations with the cc-pVDZ basis set were −199.48109 hartree and −199.48214 hartree, respectively. The error in the FMO2 calculation is thus as small as 1.1 millihartree (mh). Figure 2(a) shows the dependence of the error in the total energies on the basis sets represented by 1: STO-3G, 2: 3-21G, 3: 6-31G(d), 4: cc-pVDZ, 5: 6-311G, 6: 6-311G(d), 7: cc-pVTZ, 8: 3-21+G, and 9: 6-31++G(d,p). Figure 2(a) indicates that the error increases only slightly along the size of the basis set when the diffuse functions are excluded; however, the error starts to grow notably when the diffuse functions are involved.

Using the results of the FMO2 calculations, we then performed the FMO–LCMO calculations. The MO energy spectra calculated from the conventional HF and FMO–LCMO methods with the cc-pVDZ basis set are compared in Fig. 3. We also plot the monomer MO energy spectra $\{\epsilon_{I_p}\}$ of the (degenerate) donor/acceptor fragment and the bridge fragments. Figure 3 shows that the FMO–LCMO calculations well reproduced the MO energy spectrum of the conventional HF calculations, especially in the valence orbital range surrounded by the green dashed line. In Table I, we list the calculated maximum absolute error (MAE) and maximum relative error (MRE) of the MO energies. The MRE in Table I is defined as $|(\epsilon_{\rm conv} - \epsilon_{\rm FMO})/\epsilon_{\rm conv}|$, where $\epsilon_{\rm conv}$ and $\epsilon_{\rm FMO}$ represent the MO energies from the conventional HF and FMO–LCMO methods.

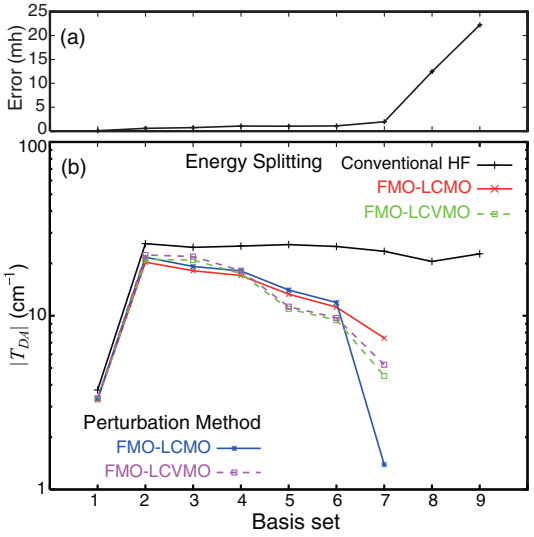

FIG. 2. Basis set dependence of (a) the errors in the total energies and (b) electronic couplings, T_{DA} in the CH_3-$(CH_4)_3$-CH_3 system. Basis set numbering is: 1 = STO-3G, 2 = 3-21G, 3 = 6-31G(d), 4 = cc-pVDZ, 5 = 6-311G, 6 = 6-311G(d), 7 = cc-pVTZ, 8 = 3-21+G, and 9 = 6-31++G(d,p).

Moreover, we performed the FMO–LCVMO calculations, by which the dimension of the FMO–LCMO total Hamiltonian were reduced from 165 to 38 at cc-pVDZ level. The monomer MOs surrounded by green dashed lines in Fig. 3 were used for such a matrix-size reduction to the valence space. As shown in Fig. 3, we found that the FMO–LCVMO calculations well reproduced the MO energy spectrum of the conventional HF calculations in the

TABLE I. Differences of MO energies and rotational angles of ψ^+ and ψ^- calculated with the FMO–LC(V)MO and conventional HF methods.

		MO energy		Rotational angle (degree)	
Molecule	Dimension	MAE[a]	MRE[b]	ψ^+	ψ^-
CH_3-$(CH_4)_3$-CH_3[c]	165	7.52×10^{-3}	1.88	3.86	2.46
	38	1.35×10^{-2}	2.65	5.54	4.52
TCNE-$(C_6H_6)_6$-TCNE[c]	1020	1.13×10^{-2}	15.1	2.62	2.62
	260	0.146	24.9	3.49	3.49
Be-$C_{10}H_{22}$-Be[d]	76				
(BDA1)		1.91×10^{-2}	7.44	44.5	44.5
(BDA2)		2.00×10^{-2}	5.32	0.628	0.628

[a]Maximum absolute error (hartree).
[b]Maximum relative error (%).
[c]The cc-pVDZ basis set was used.
[d]The MINI basis set was used.

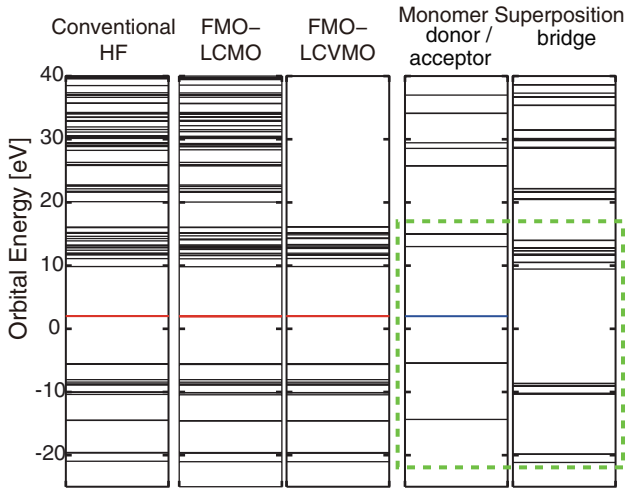

FIG. 3. Canonical MO energy spectra obtained from the conventional HF, full-size FMO–LCMO, and FMO–LCVMO methods with the cc-pVDZ basis set in the CH_3-$(CH_4)_3$-CH_3 system. Superposed MO energy spectra obtained from the FMO2 calculations for each (degenerate) donor/acceptor monomer fragment (CH_3) and each bridge fragment (CH_4) are also plotted.

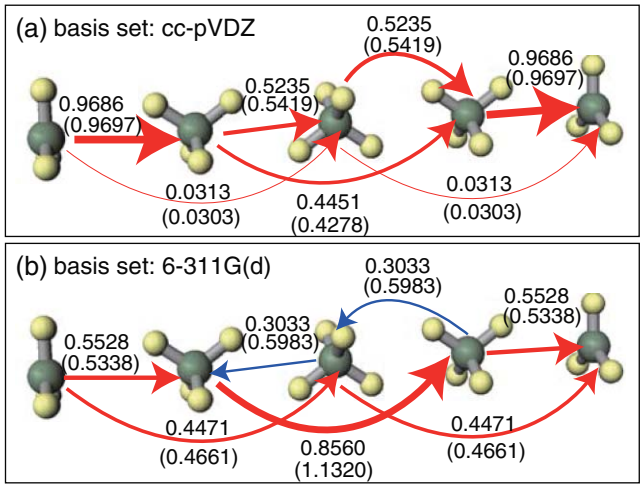

FIG. 4. Maps of normalized inter-fragment tunneling currents $K_{L,M}$ obtained for the CH_3-$(CH_4)_3$-CH_3 system with (a) the cc-pVDZ and (b) 6-311G(d) basis sets. The arrows represent the $K_{L,M}$'s, with the thickness roughly proportional to their absolute value. The numerical figure near each arrow stands for its $|K_{L,M}|$ value from the FMO–LCMO calculation, and the figure in parentheses is the corresponding value from the FMO–LCVMO calculation.

corresponding valence orbital region. In Table I, we also list the MAE and MRE of the MO energies from the FMO–LCVMO calculations.

We next calculated the $|T_{DA}|$ values by using Eq. (8) with the conventional HF, FMO–LCMO, and FMO–LCVMO calculations. In Fig. 3, the red lines represent the two energies (ϵ_+ and ϵ_-) of the quasi-degenerate HOMO-1 (ψ^+) and HOMO (ψ^-) used in Eq. (8). To examine the difference of the obtained MO shape, we calculated the rotational angles of ψ^+ and ψ^- defined as

$$\cos^{-1}\frac{C^{\pm}_{\mathrm{FMO}}\cdot C^{\pm}_{\mathrm{conv}}}{|C^{\pm}_{\mathrm{FMO}}||C^{\pm}_{\mathrm{conv}}|}, \tag{17}$$

where $C^{\pm}_{\mathrm{FMO}}$ and $C^{\pm}_{\mathrm{conv}}$ represent the MO coefficient vector of $\psi^{\pm}$ in atomic orbital representation calculated with the FMO–LCMO and conventional HF methods, respectively. The small rotational angles of ψ^+ and ψ^- shown in Table I indicate that the FMO–LCMO calculations reproduced the proper tunneling orbitals. In Fig. 2(b), we plot the $|T_{DA}|$ values obtained from the conventional HF (black), FMO–LCMO (red), and the FMO–LCVMO (dashed green) calculations, as functions of the basis sets. The $|T_{DA}|$ value from conventional HF method did not depend much on the basis set except for the STO-3G. Comparing with the conventional HF calculations, we can see that both the FMO–LCMO and FMO–LCVMO calculations reasonably reproduce the reference $|T_{DA}|$ value, although the deviation gradually increases along the size of the basis set. When using diffuse-function basis set, the HOMO-1 and HOMO from the FMO–LC(V)MO calculations were not in the appropriate form for ψ^+ and ψ^-. This is likely due to the so-called "discrete" continuum states effect known for the cases involving diffuse-functions.[31,37]

Next, we calculated the $|T_{DA}|$ values by using perturbation method Eq. (9) with the FMO–LCMO and FMO–LCVMO calculations. The HOMOs obtained for the donor and acceptor fragments were set to ϕ_D and ϕ_A, respectively. In Fig. 3, the blue line represents the MO energy of the degenerate ϕ_D and ϕ_A obtained with the cc-pVDZ basis set. (This energy, 1.986 eV, was therefore used for E_{tun} in the case of this basis set.) In Fig. 2(b), we plot the $|T_{DA}|$ values from the FMO–LCMO (blue) and the FMO–LCVMO (dashed purple). Figure 2(b) shows that the $|T_{DA}|$'s from Eq. (9) (blue) agree well with those from Eq. (8) (red) in the FMO–LCMO calculation except for the cc-pVTZ basis set. Figure 2(b) also shows that the FMO–LCVMO calculation gives good agreement between Eq. (9) (dashed purple) and Eq. (8) (dashed green).

In Fig. 4, we draw the normalized inter-fragment tunneling-currents $K_{L,M}$'s, using Eq. (16) with (a) cc-pVDZ and (b) 6-311G(d) basis sets, respectively. The red arrows represent the $K_{L,M}$'s flowing from donor to acceptor. The blue arrows represent the $K_{L,M}$'s flowing back from the acceptor to donor, leading to the destructive interference. The numerical figure near the arrow stands for its $|K_{L,M}|$ value from the FMO–LCMO calculation. The figure in parentheses stands for the corresponding $|K_{L,M}|$ value from the FMO–LCVMO calculation. As shown in Fig. 4(b), the $K_{L,M}$ map with the 6-311G(d) basis set indicates that the destructive interference occurs in contrast to that with the cc-pVDZ basis set. With the cc-pVDZ basis set, the $K_{L,M}$ maps from the FMO–LCMO and FMO–LCVMO calculations are highly consistent with each other. However, this is not the case with the 6-311G(d) basis set, where the matrix-size reduction affected the $K_{L,M}$ values among the bridge fragments, leading to enhancement of the destructive interference.

B. TCNE-$(C_6H_6)_n$-TCNE systems

We now carry out similar analysis on TCNE-$(C_6H_6)_n$-TCNE. We first performed both the conventional HF and FMO2 calculations with the cc-pVDZ basis set.[92] The errors between the conventional HF and FMO2 total energies were from 0.044 mh ($n = 1$) to 1.2 mh ($n = 8$).

Using the results of the FMO2 calculations, we then performed the FMO–LCMO calculations. We found that the FMO–LCMO calculations well reproduced the MO energy spectrum of the conventional HF calculations, especially in the valence orbital region. We also performed FMO–LCVMO calculations by which the dimension of the FMO–LCMO total Hamiltonian were reduced from 1020 to 260. We found that the FMO–LCVMO calculations well reproduced the MO energy spectrum of the conventional HF calculations in the valence orbital region. The MO energy spectra from the conventional HF, FMO–LCMO, and FMO–LCVMO calculations for the TCNE-$(C_6H_6)_6$-TCNE are plotted in Fig. S1 in the supplementary material (SM).[94] The monomer MO energy spectra for the TCNE-$(C_6H_6)_6$-TCNE are also plotted in Fig. S1 in SM.[94] In Table I, we list the MAE and MRE of the MO energies of the TCNE-$(C_6H_6)_6$-TCNE calculated with the cc-pVDZ basis set.

We next calculated the $|T_{DA}|$ values by using Eq. (8) with the conventional HF, FMO–LCMO, and FMO–LCVMO calculations. The two energies (ϵ_+ and ϵ_-) of the quasi-degenerate LUMO (ψ^+) and LUMO+1 (ψ^-) were used. The results are plotted in Fig. 5(a) for the conventional HF (black), FMO–LCMO (red), and FMO–LCVMO (green) as functions of the number of benzene molecules. As shown, the calculated $|T_{DA}|$ values decreased exponentially with increasing n. The $|T_{DA}|$ values calculated with the cc-pVDZ basis set decreased with increasing n more gradually than those calculated with the 3-21G basis set, plotted in Fig. S2 in SM.[94] In Fig. 5(b), we plot the ratio $T_{DA}^{\mathrm{FMO}}/T_{DA}^{\mathrm{conv}}$ for full FMO–LCMO (red) and FMO–LCVMO (green), respectively. As shown, we can see that both the FMO–LCMO and FMO–LCVMO calculations produced reasonable $|T_{DA}|$ values in the range of $n = 1$ to 8. In Table I, we list the rotational angles of ψ^+ and ψ^- of TCNE-$(C_6H_6)_6$-TCNE obtained from Eq. (17) with the cc-pVDZ basis set.

We also calculated the $|T_{DA}|$ values by using perturbation method Eq. (9) with the FMO–LCMO and FMO–LCVMO calculations. The LUMOs obtained for the donor and acceptor fragments were set to ϕ_D and ϕ_A, respectively. In Fig. 5, we plot the $|T_{DA}|$ values from the FMO–LCMO (broken blue) and the FMO–LCVMO (broken purple). Figure 5 shows that the perturbative results from Eq. (9) well reproduced the $|T_{DA}|$ values from the energy-splitting Eq. (8) in this system.

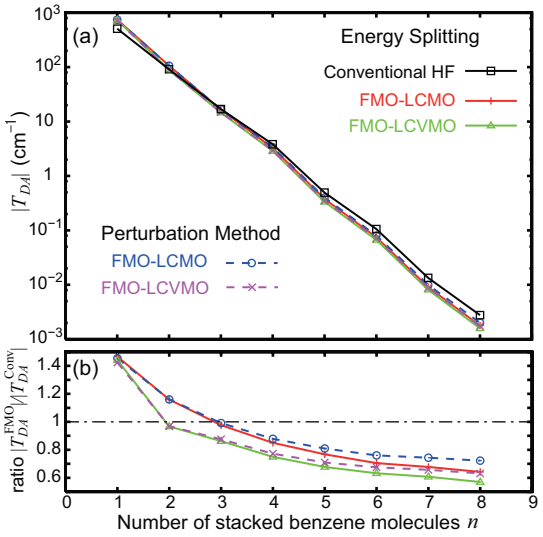

FIG. 5. (a) Dependence of $|T_{DA}|$ on the number of stacked benzene molecules n in the TCNE-$(C_6H_6)_n$-TCNE system calculated with the cc-pVDZ basis set. (b) Dependence of the ratio $|T_{DA}^{\mathrm{FMO}}|/|T_{DA}^{\mathrm{conv}}|$ on n.

C. Be-C_nH_{2n+2}-Be systems

We now proceed to the systems in which the bridge fragments are covalently connected and thus the BDAs are involved. We first performed the conventional HF and FMO2 calculations for Be-C_nH_{2n+2}-Be systems. For the MO purification required for the FMO–LCMO method, we used the minimal basis set MINI,[95] see Sec. II A. In the FMO2 calculations, we employed the two methods, BDA1 and BDA2, as described in Sec. III B.

In Fig. 6(a) we plot the error between the total energies calculated from the conventional HF and FMO2 with BDA1 (red) and BDA2 (green) as a function of n (the number of carbon atoms of alkanes). Figure 6(a) shows that both the errors increased linearly with increasing n in the regions where the bond-detached atoms were used ($n \geq 4$ for BDA1 and $n \geq 6$ for BDA2, respectively). Figure 6(a) also shows that the FMO2 calculations with BDA2 produced less errors in the total energy than those with BDA1. Although the minimal

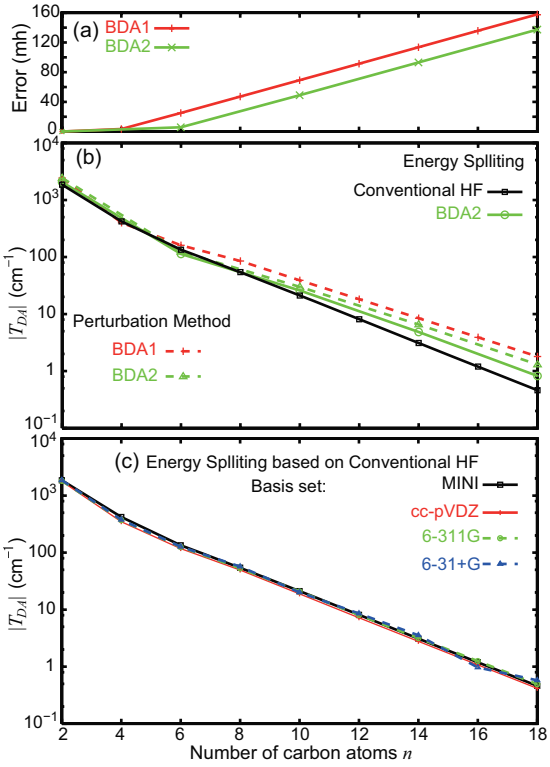

FIG. 6. (a) Dependences of the errors between the total energies from the conventional HF and FMO2 calculations on the number of carbon atoms n in the Be-C_nH_{2n+2}-Be system calculated with the MINI basis set. (b) Dependences of T_{DA} on n calculated from the energy splitting (solid lines) and from the perturbation method (dashed lines) with the MINI basis set. The red and green lines represent the results from the FMO–LCMO calculations with the BDA1 and BDA2 methods for bond-detached atoms, respectively. (c) Dependences of T_{DA} on n calculated from the conventional HF with the MINI (black), cc-pVDZ (red), 6-311G (dashed green), and 6-31+G (dashed blue) basis sets, respectively.

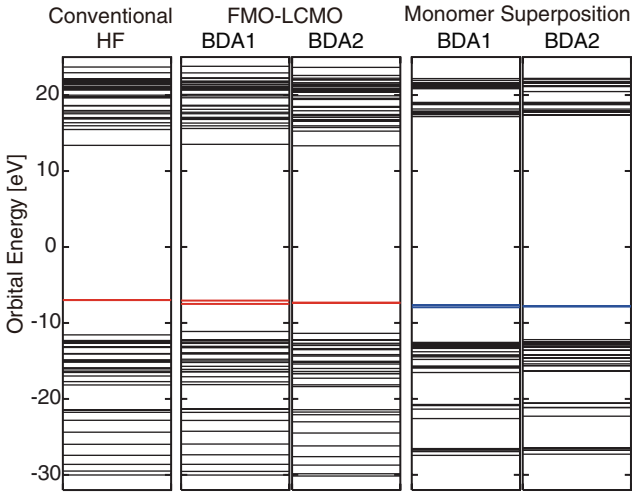

FIG. 7. Canonical MO energy spectra obtained from the conventional HF and FMO–LCMO with BDA1 and BDA2 for the Be-$C_{10}H_{22}$-Be system. Superposed MO energy spectra of each MO energy spectrum of the monomer fragment in the FMO2 calculation with the BDA1 and BDA2 methods are also plotted.

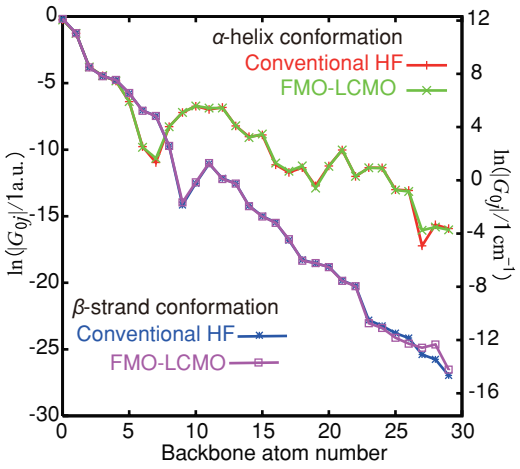

FIG. 8. Green function matrix elements between 2*s* atomic orbital of the first amide nitrogen atom and 2*s* atomic orbitals of the other backbone atoms in ala_{10} calculated from the conventional HF and FMO–LCMO methods with the MINI basis set.

basis set was used for such a small system, the error between the total energies was rather large (compare with Fig. 2(a)).

Using the results of the FMO2 calculations, we then performed the FMO–LCMO calculations. The MO energy spectra obtained from the conventional HF, FMO–LCMO with BDA1, and FMO–LCMO with BDA2 for the Be-$C_{10}H_{22}$-Be system are compared in Fig. 7. In Table I, we list the MAE and MRE of the MO energies of the Be-$C_{10}H_{22}$-Be. The superposed MO energy spectra of the monomer fragments calculated from the FMO–LCMO with BDA1 and BDA2 are also plotted in Fig. 7. By construction, the FMO2 calculations with BDA1 did not produce the monomer and dimer solutions that reflect the C_{2h} symmetry of the entire system. This broken symmetry is therefore carried over to the FMO–LCMO calculations. In Fig. 7, the blue lines are the HOMOs obtained for the donor and acceptor fragments (i.e., the terminal Be atoms) and adopted as ϕ_D and ϕ_A in the T_{DA} calculations. As shown, ϕ_D and ϕ_A obtained with BDA1 were not degenerated. In Fig. 7, the red lines are the HOMO-1 and HOMO adopted as ψ^+ and ψ^- in the T_{DA} calculations. The ψ^+ and ψ^- obtained with BDA1 were localized on the donor and acceptor Be atoms, respectively, and as a result the T_{DA} could not be calculated from its energy splitting Eq. (8). In contrast, the FMO–LCMO calculations with BDA2 produced the solutions reflecting the C_{2h} symmetry of the molecule. In Table I, we list the rotational angles of ψ^+ and ψ^- of Be-$C_{10}H_{22}$-Be obtained from Eq. (17).

In Fig. 6(b) we plot the calculated T_{DA} values as a function of n. The solid and dashed lines represent the results from the energy splitting Eq. (8) and from the perturbation method Eq. (9), respectively. The black, red, and green lines represent the results from the conventional HF, FMO–LCMO with BDA1, and FMO–LCMO with BDA2, respectively. As shown, the obtained T_{DA} values decreased exponentially with increasing n, reflecting the nature of superexchange tunneling. Comparing with the conventional HF, the FMO–LCMO calculations reproduced the reasonable T_{DA} values even though the error in the total energy was as large as seen in Fig. 6(a).

In Fig. 6(c), we plot the calculated T_{DA} values from the conventional HF method with several basis sets. In this system, the calculated T_{DA} did not depend much on the employed basis sets.

D. ala_{10} systems

Here, we show the results of the isolated Green function matrix, Eq. (10), obtained for the ala_{10} systems having the idealized α-helix and β-strand conformations. As in Sec. IV C, we used the MINI basis set.[95]

The total energies calculated from the conventional HF and FMO2 calculations were −2442.44389 hartree and −2442.44382 hartree for α-helix conformation, and −2442.39331 hartree and −2442.39332 hartree for β-strand conformation, respectively. The errors in the FMO2 calculations are thus as small as 0.071 mh for α-helix conformation and 0.010 mh for β-strand conformation. To obtain the Green function matrix, we performed the FMO–LCMO calculations with the matrix-size reduction where the core orbitals in monomer MOs and dimer MOs were eliminated from Eqs. (3)–(5). Figure 8 shows the results of the Green function matrix elements between the 2*s* atomic orbital of the first amide nitrogen atom and the 2*s* atomic orbitals of the other backbone atoms. In these calculations, the tunneling energy E_{tun}, in Eq. (10), was set to −3.0 eV. As shown, we found that the Green function matrix elements from the FMO–LCMO method were in good agreement with those from the conventional HF method in all ranges for both the α-helix and β-strand ala_{10} systems. We also plotted the Green function matrix elements with $E_{\text{tun}} = -5.0$ eV and $E_{\text{tun}} = -1.0$ eV in Fig. S3 in the SM.[94]

V. DISCUSSION

In this study, we have calculated the T_{DA} or Green function matrix elements for the four model ET systems in

terms of the FMO–LCMO Hamiltonian matrix. As shown in Figs. 2(b), 5, 6(b), and 8, we obtained the reasonable results agreeing with those form the conventional HF method. Here we shall discuss reasons why the FMO–LCMO method was applicable to these calculations in long-distance ETs. Within the context of the HF-KT scheme, the electron tunneling can be described by the ψ^i and ψ^f (degenerate diabatic states) or their symmetric and antisymmetric mixing MOs, ψ^+ and ψ^- (quasidegenerate adiabatic states). In long-distance ETs, ψ^i and ψ^f are mostly localized at the donor and acceptor sites with exponentially small "tail" in the bridge region. The native FMO method cannot produce the tails spreading over whole bridge fragments because the electrons are rigidly assigned to each fragment. On the other hand, the diagonalization of the FMO–LCMO Hamiltonian matrix (or perturbation method using Eq. (9)) effectively takes into account the electronic interactions among fragments, thereby reproducing the tails of ψ^i and ψ^f. Since the T_{DA} arising from overlap between the tails is as small or less than 100 cm^{-1}, perturbative approaches are appropriate.[9,96] Therefore, the energy splitting Eq. (8) and perturbation method Eq. (9) in terms of the FMO–LCMO Hamiltonian matrix could indeed produce the reasonable T_{DA}.

The notably attractive feature of the FMO–LCMO method is that limiting the monomer MOs expanding the matrices Eqs. (3) and (5) can reduce the size of the total Hamiltonian matrix Eqs. (6) and (7).[85] For typical biological systems, constructing and diagonalizing the total Hamiltonian matrix after the FMO calculation demand computational costs much larger than the FMO calculation itself.[97] Since the electron tunneling is mainly described by the ψ^+ and ψ^- or ψ^i and ψ^f whose energies are located at about the center of HOMO-LUMO gap of bridge MO energies (see Figs. 3 and 7), and the perturbative approaches are appropriate as discussed above, one can expect that it is sufficient to deal with narrow range of MO energy spectrum corresponding to the valence MO space. In this study, we took into account the valence monomer MOs in Eqs. (3) and (5) for the size reduction. The dimer Hamiltonian Eq. (5) expanded by the valence monomer MOs effectively included the effects of the extra-valence dimer MOs. As shown in Figs. 2, 5, and 8, both Eqs. (8) and (9) with the FMO–LCVMO method produced the reasonable T_{DA} in comparison with those with the full-size FMO–LCMO method. Figure 4 shows the FMO–LCVMO method also produced the reasonable $K_{L,M}$ map in comparison with the full-size one. The previous works[55,56,58,62,63,84] have also succeeded in the T_{DA} calculations in terms of the effective Hamiltonian matrix projected to the valence atomic orbital space. Such size-reduction procedures will be essential for studying the realistic protein ETs.

To approximate the T_{DA}, we used the perturbation method Eq. (9) in which the frontier MO (HOMO or LUMO) obtained for donor/acceptor fragment was adopted as the zeroth-order donor/acceptor orbital ϕ_D/ϕ_A and all the other monomer MOs were adopted as the bridge orbitals. In general, the choice of donor, acceptor, and bridge states from the conventional canonical MOs is not unique and such ambiguity can cause difficulties to describe the electron tunneling correctly.[9,17,19] In contrast, the FMO calculation is designed to produce monomer MOs as charge-localized zeroth-order orbitals. As shown in Figs. 2(b), 5, and 6(b), the T_{DA} values from Eq. (9) with the monomer MO representation were in reasonable agreement with those from Eq. (8). The perturbation method will play more important role to evaluate T_{DA} for realistic protein ET systems because the calculation of energy splitting Eq. (8) might have potential practical problems as follows:[9,96] (1) The T_{DA} value as small as 10^{-1} cm^{-1} for typical protein ET systems should be calculated from the difference of two large values ϵ_+ and ϵ_- in Eq. (8). (2) Since typical protein ET systems do not have symmetric donor-bridge-acceptor configuration, it is not a trivial task to find the avoided crossing point with accuracy of less than 10^{-1} cm^{-1} by use of the external charge or field. This last issue is described later in this section. The numerical difficulties in calculating realistically small T_{DA} (e.g., less than 10^{-2} cm^{-1}), including the above problems (1) and (2), were well discussed in Refs. 9 and 60. As described in the first paragraph of this section, the nature of the "tails" of ψ^i and ψ^f can be reproduced by the FMO–LCMO method. Therefore, our approach is well expected to reproduce reliable results for systems where T_{DA} is realistically small; indeed, this was demonstrated for the TCNE-$(C_6H_6)_n$-TCNE systems in the regions of 10^{-2}-10^{-3} cm^{-1} (Fig. 5). Tests on realistic ET proteins will be reported in due course.

In this study, we have used the normalized inter-fragment tunneling current $K_{L,M}$ to analyze and visualize the tunneling pathway. In FMO calculation for biological system, the protein is generally divided into fragments where one or two amino acid residues are taken as a fragment.[71] Therefore, our $K_{L,M}$ has amino acid resolution, expressing the rather coarse-grained tunneling pathway compared with the interatomic tunneling currents;[9,18,19,21,22,42,43] we consider this resolution can be advantageous for many purposes, e.g., to determine the important amino acids for long-distance electron tunneling in biological ET systems. Moreover, one can improve $K_{L,M}$ to take into account the effect of the fluctuating protein structure by following the previous study.[98]

For the CH_3-$(CH_4)_3$-CH_3 system, we calculated the T_{DA} values with several basis sets. The FMO2 total energies calculated with the triple-zeta and diffuse-function basis sets were in poor agreement with the conventional HF energies, as shown in Fig. 2(a). This would be partly because the chosen fragment size, i.e., one CH_3 or CH_4 molecule, was too small and rather incompatible with the choice of these large basis sets. As a result, the FMO–LCMO calculations with the triple-zeta basis sets produced the T_{DA} values much smaller than the conventional HF calculations in comparison with those with the minimal and double-zeta basis sets, as shown in Fig. 2(b). These underestimations can be explained by the inter-fragment tunneling current $K_{L,M}$ as follows: In comparison with the $K_{L,M}$ map with the cc-pVDZ basis set in Fig. 4(a), we can see that the $K_{L,M}$ map with the 6-311G(d) basis set in Fig. 4(b) shows the destructive interference occurring among the $K_{L,M}$'s represented by red and blue arrows. This may lead to the underestimation of the T_{DA} values calculated with the triple-zeta basis sets. The underestimation of T_{DA} from the size-reduction FMO–LCVMO method in comparison with the full-size FMO–LCMO calculation is also

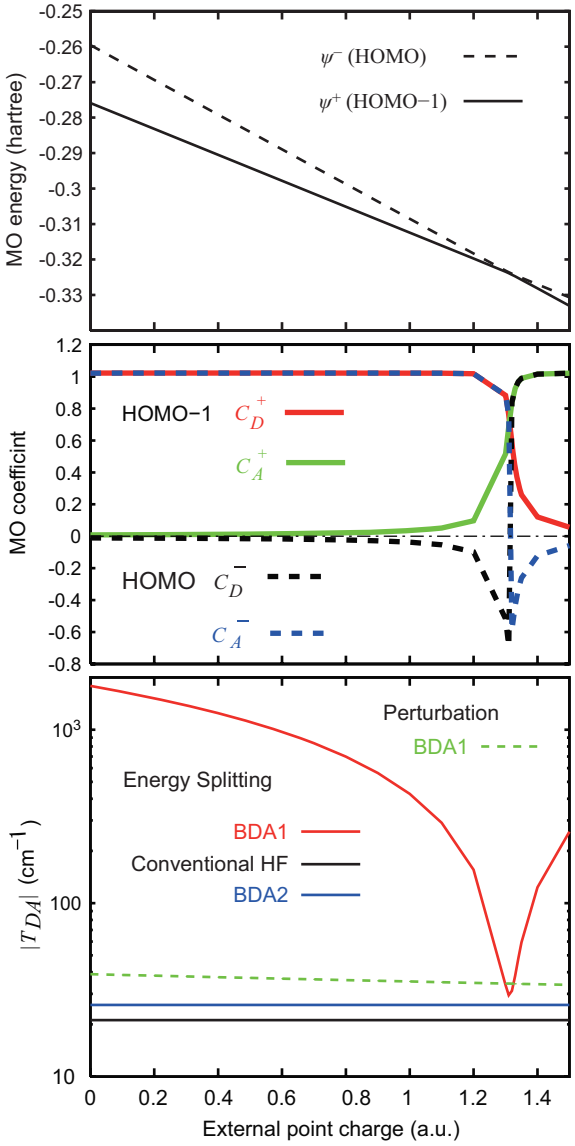

FIG. 9. Dependences of (a) MO energies of ψ^+ and ψ^- and (b) their MO coefficients with respect to ϕ_D and ϕ_A obtained from the FMO–LCMO calculations with the BDA1 method and the MINI basis set on the external point charge in the Be-$C_{10}H_{22}$-Be system. (c) The $|T_{DA}|$ values with BDA1 from the energy splitting (red) and perturbation (dashed green) as a function of the external point charge. For comparison, the $|T_{DA}|$ values from the conventional HF and the FMO–LCMO with BDA2 without the point charge are also indicated by the solid black and blue horizontal lines, respectively.

explained by the enhancement of the destructive interference shown in Fig. 4(b).

In the Be-C_nH_{2n+2}-Be systems, the FMO–LCMO calculations with the BDA1 did not produce the proper quasidegenerate ψ^+ and ψ^- because the way to distribute the NLMOs on the BDAs broke the symmetry of the system. As a result, T_{DA} could not be calculated from the energy splitting Eq. (8). Naturally, the realistic ET systems do not necessarily have such symmetric donor-bridge-acceptor configuration, and the electron tunneling occurs when the ψ^+ and ψ^- are brought into the avoided crossing by the thermal fluctuation of the molecular environment. To imitate such environmental effect, external charges or field has been applied in many previous studies.[6,9,19,26–29,55,58,60] Our approach based on the FMO–LCMO method can utilize the external charge or field without any technical problem and with only fractional computational cost since the electronic structure calculation of each fragment already includes the Coulomb field of all other fragments in the FMO method. To confirm this, an external positive charge was placed at 3 Å away from the donor Be atom on the line connecting the two Be atoms in the Be-$C_{10}H_{22}$-Be system (see Fig. 1(c)). In Fig. 9, we plot the MO energies of ψ^+ and ψ^- as well as their MO coefficient with respect to ϕ_D and ϕ_A obtained from the FMO–LCMO calculation with BDA1 as a function of the magnitude of the external point charge Q. Figures 9(a) and 9(b) indicate that the avoided crossing happens at about $Q = 1.31$ a.u. In Fig. 9(c), we plot the T_{DA}s obtained from Eq. (8) (red) and from Eq. (9) (broken green) as a function of Q. For comparison, we also include as horizontal lines the half-energy splitting values from the conventional HF (black) and FMO–LCMO with BDA2 (blue) calculated without the external point charge. Figure 9(c) shows that the red line well approaches the blue and black lines at about $Q = 1.31$ a.u.

VI. CONCLUSIONS

We have proposed a novel approach to calculate T_{DA} and the tunneling pathway by making use of the FMO–LCMO method. In our approach, T_{DA} can be calculated from the MO energy splitting Eq. (8) and from the perturbation method Eq. (9) in terms of the FMO–LCMO Hamiltonian matrix. Our approach was tested on the four different types of model systems, CH_3-$(CH_4)_3$-CH_3, TCNE-$(C_6H_6)_n$-TCNE, Be-C_nH_{2n+2}-Be, and ala_{10} in the idealized α-helix and β-strand conformations. As a result, we obtained the reasonable T_{DA} and $G^B(E_{\text{tun}})$ for all cases, as shown in Figs. 2(b), 5, 6(b), and 8. We also obtained the tunneling pathway from the $K_{L,M}$ map in terms of the FMO–LCMO Hamiltonian matrix, as shown in Fig. 4.

The features of our approach are summarized as follows:

- Limiting the number of monomer MOs in expanding the matrices Eqs. (3) and (5) can reduce the size of the FMO–LCMO Hamiltonian matrix Eqs. (6) and (7). The matrix-size reduction considerably reduces the computational cost for both constructing and diagonalizing the Hamiltonian matrix, which is expected to be particularly advantageous for realistic biological systems.
- Perturbation method Eq. (9) in terms of the FMO–LCMO matrix in the monomer MO representation is expected to be more robust numerically than the energy splitting Eq. (8) for calculating small T_{DA}-values in large systems.
- The external charge or field can be used to find the avoided crossing point with almost negligible additional computational cost and in a straightforward manner because it is already compatible with the FMO calculation.

Although the four model systems employed in this study have the homogeneous bridges, our approach foresees no particular obstacle for application to realistic large systems with

inhomogeneous bridges because of the above reasons. To obtain reliable computational results under the real experimental situations, we should take into account the effects of thermal fluctuation of the ET systems and electrostatic interactions between donor-bridge-acceptor and solvent in addition to searching the transition state conformation. The application for addressing these important issues in biological ET systems will be reported in the future paper of this series of study.

ACKNOWLEDGMENTS

The authors acknowledge support from KAKENHI on Innovative Areas (No. 20108017, "π-space").

[1]H. M. McConnel, J. Chem. Phys. **35**, 508 (1961).
[2]C. C. Moser, J. M. Keske, K. Warncke, R. S. Farid, and P. L. Dutton, Nature **355**, 796 (1992).
[3]R. A. Marcus and N. Sutin, Biochim. Biophys. Acta **811**, 265 (1985).
[4]M. Bixon and J. Jortner, Adv. Chem. Phys. **106**, 35 (1999).
[5]H. B. Gray and J. R. Winkler, Proc. Natl. Acad. Sci. U.S.A. **102**, 3534 (2005).
[6]M. D. Newton, Chem. Rev. **91**, 767 (1991).
[7]S. S. Skourtis and D. N. Beratan, Adv. Chem. Phys. **106**, 377 (1999).
[8]J. J. Regan and J. N. Onuchic, Adv. Chem. Phys. **107**, 497 (1999).
[9]A. A. Stuchebrukhov, Theor. Chem. Acc. **110**, 291 (2003).
[10]D. N. Beratan, J. N. Betts, and J. N. Onuchic, Science **252**, 1285 (1991).
[11]D. N. Beratan, J. N. Betts, and J. N. Onuchic, J. Phys. Chem. **96**, 2852 (1992).
[12]J. J. Regan, S. M. Risser, D. N. Beratan, and J. N. Onuchic, J. Phys. Chem. **97**, 13083 (1993).
[13]C. C. Page, C. C. Moser, X. Chen, and P. L. Dutton, Nature **402**, 47 (1999).
[14]M. L. Jones, I. V. Kurnikov, and D. N. Beratan, J. Phys. Chem. A **106**, 2002 (2002).
[15]J. M. Gruschus and A. Kuki, J. Phys. Chem. **97**, 5581 (1993).
[16]P. Siddarth and R. A. Marcus, J. Phys. Chem. **97**, 2400 (1993).
[17]A. A. Stuchebrukhov and R. A. Marcus, J. Phys. Chem. **99**, 7581 (1995).
[18]A. A. Stuchebrukhov, J. Chem. Phys. **105**, 10819 (1996).
[19]I. Daizadeh, J. N. Gehlen, and A. A. Stuchebrukhov, J. Chem. Phys. **106**, 5658 (1997).
[20]A. Okada, T. Kakitani, and J. Inoue, J. Phys. Chem. **99**, 2946 (1995).
[21]T. Kawatsu, T. Kakitani, and T. Yamato, Inorg. Chim. Acta. **300–302**, 862 (2000).
[22]T. Kawatsu, T. Kakitani, and T. Yamato, J. Phys. Chem. B **105**, 4424 (2001).
[23]M. Plato, M. E. Michel-Beyerle, M. Bixon, and J. Jortner, FEBS Lett. **249**, 70 (1989).
[24]S. Priyadarshy, S. M. Risser, and D. N. Beratan, J. Phys. Chem. **100**, 17678 (1996).
[25]S. S. Skourtis and D. N. Beratan, J. Phys. Chem. B **101**, 1215 (1997).
[26]N. Ivashin, B. Källebring, S. Larsson, and O. Hansson, J. Phys. Chem. B **102**, 5017 (1998).
[27]S. Larsson and N. V. Ivashin, J. Appl. Spectrosc. **66**, 539 (1999).
[28]X. H. Zheng and A. A. Stuchebrukhov, J. Phys. Chem. B **107**, 6621 (2003).
[29]T. Hayashi and A. A. Stuchebrukhov, Proc. Natl. Acad. Soc. U.S.A. **107**, 19157 (2010).
[30]C. Liang and M. D. Newton, J. Phys. Chem. **97**, 3199 (1993).
[31]L. A. Curtiss, C. A. Naleway, and J. R. Miller, J. Phys. Chem. **97**, 4050 (1993).
[32]K. D. Jordan and M. N. Paddon-Row, Chem. Rev. **97**, 395 (1992).
[33]S. Hayashi and S. Kato, J. Phys. Chem. A **102**, 2878 (1998).
[34]M. Lee, M. J. Shephard, S. M. Risser, S. Priyadarshy, M. N. Paddon-Row, and D. N. Beratan, J. Phys. Chem. A **104**, 7593 (2000).
[35]A. Teklos and S. S. Skourtis, J. Chem. Phys. **125**, 244103 (2006).
[36]C.-P. Hsu, Acc. Chem. Res. **42**, 509 (2009).
[37]H. Nishioka and K. Ando, Phys. Chem. Chem. Phys. **13**, 7043 (2011).
[38]J. Wolfgang, S. M. Risser, S. Priyadarshy, and D. N. Beratan, J. Phys. Chem. B **101**, 2986 (1997).
[39]I. Daizadeh, E. S. Medvedev, and A. A. Stuchebrukhov, Proc. Natl. Acad. Sci. U.S.A. **94**, 3703 (1997).
[40]Q. Xie, G. Archontis, and S. S. Skourtis, Chem. Phys. Lett. **312**, 237 (1999).
[41]I. A. Balabin and J. N. Onuchic, Science **290**, 114 (2000).
[42]T. Kawatsu, T. Kakitani, and T. Yamato, J. Phys. Chem. B **106**, 11356 (2002).
[43]H. Nishioka, A. Kimura, T. Yamato, T. Kawatsu, and T. Kakitani, J. Phys. Chem. B **109**, 1978 (2005).
[44]Y. Miyazawa, H. Nishioka, K. Yura, and T. Yamato, Biophys. J. **94**, 2194 (2008).
[45]H. Nishioka, N. Ueda, and T. Kakitani, Biophysics **4**, 19 (2008).
[46]I. A. Balabin, D. N. Beratan, and S. S. Skourtis, Phys. Rev. Lett. **101**, 158102 (2008).
[47]M. Bixon and J. Jortner, Russ. J. Electronchem. **39**, 3 (2003).
[48]A. Troisi, A. Nitzan, and M. A. Ratner, J. Chem. Phys. **119**, 5782 (2003).
[49]S. S. Skourtis, I. A. Balabin, T. Kawatsu, and D. N. Beratan, Proc. Natl. Acad. Sci. U.S.A. **102**, 3552 (2005).
[50]H. Nishioka, A. Kimura, T. Yamato, T. Kawatsu, and T. Kakitani, J. Phys. Chem. B **109**, 15621 (2005).
[51]S. Tanaka and E. B. Starikov, Phys. Rev. E **81**, 027101 (2010).
[52]D. N. Beratan, S. S. Skourtis, I. A. Balabin, A. Balaeff, S. Keinan, R. Venkatramani, and D. Xiao, Acc. Chem. Res. **42**, 1669 (2009).
[53]S. S. Skourtis, D. H. Waldeck, and D. N. Beratan, Annu. Rev. Phys. Chem. **61**, 461 (2010).
[54]C. Kobayashi, K. Baldridge, and J. N. Onuchic, J. Chem. Phys. **119**, 3550 (2003).
[55]T. R. Prytkova, I. V. Kurnikov, and D. N. Beratan, J. Phys. Chem. B **109**, 1618 (2005).
[56]T. R. Prytkova, I. V. Kurnikov, and D. N. Beratan, Science **315**, 622 (2007).
[57]A. Migliore, S. Corni, R. D. Felice, and E. Molinari, J. Phys. Chem. B **111**, 3774 (2007).
[58]M. R. Hartings, I. V. Kurnikov, A. R. Dunn, J. R. Winkler, H. B. Gray, and M. A. Ratner, Coord. Chem. Rev. **254**, 248 (2010).
[59]L. Y. Zhang and R. A. Friesner, Proc. Natl. Acad. Sci. U.S.A. **95**, 13603 (1998).
[60]J. Kim and A. A. Stuchebrukhov, J. Phys. Chem. B **104**, 8606 (2000).
[61]H. Ito and H. Nakatsuji, J. Comput. Chem. **22**, 265 (2001).
[62]I. V. Kurnikov and D. N. Beratan, J. Chem. Phys. **105**, 9561 (1996).
[63]E. Babini, I. Bertini, M. Borsari, F. Capozzi, C. Luchinat, X. Zhang, G. L.C. Moura, I. V. Kurnikov, D. N. Beratan, A. Ponce, A. J. D. Bilio, J. R. Winkler, and H. B. Gray, J. Am. Chem. Soc. **122**, 4532 (2000).
[64]S. Goedecker, Rev. Mod. Phys. **71**, 1085 (1999).
[65]S. Y. Wu and C. S. Jayanthi, Phys. Rep. **358**, 1 (2002).
[66]D. G. Fedorov and K. Kitaura, J. Phys. Chem. A **111**, 6904 (2007).
[67]A. Imamura, Y. Aoki, and K. Maekawa, J. Chem. Phys. **95**, 5419 (1991).
[68]J. J. P. Stewart, Int. J. Quantum Chem. **58**, 133 (1996).
[69]K. Kitaura, E. Ikeo, T. Asada, T. Nakano, and M. Uebayasi, Chem. Phys. Lett. **313**, 701 (1999).
[70]T. Nakano, T. Kaminuma, T. Sato, Y. Akiyama, M. Uebayasi, and K. Kitaura, Chem. Phys. Lett. **318**, 614 (2000).
[71]D. G. Fedorov and K. Kitaura, J. Chem. Phys. **120**, 6832 (2004).
[72]H. Kashiwagi, H. Iwai, K. Tokieda, M. Era, T. Sumita, T. Yoshihiro, and F. Sato, Mol. Phys. **101**, 81 (2003).
[73]D. W. Zhang and J. Z.H. Zhang, J. Chem. Phys. **119**, 3599 (2003).
[74]G. P. Das, A. T. Yeates, and D. S. Dudis, Int. J. Quantum Chem. **92**, 22 (2003).
[75]W. Yang, Phys. Rev. Lett. **66**, 1438 (1991).
[76]W. Yang and T.-S. Lee, J. Chem. Phys. **103**, 5674 (1995).
[77]T. Akama, M. Kobayashi, and H. Nakai, J. Comput. Chem. **28**, 2003 (2007).
[78]T. Akama, A. Fujii, M. Kobayashi, and H. Nakai, Mol. Phys. **105**, 2799 (2007).
[79]T. Akama, M. Kobayashi, and H. Nakai, Int. J. Quantum Chem. **109**, 2706 (2009).
[80]P. O. Lowdin, J. Mol. Spectrosc. **10**, 12 (1963).
[81]P. O. Lowdin, J. Math. Phys. **6**, 1341 (1965).
[82]R. Zwanzig, *Lectures in Theoretical Physics* (Interscience, New York, 1961), Vol. 3.
[83]I. V. Kurnikov, L. D. Zusman, M. G. Kurnikova, R. S. Farid, and D. N. Beratan, J. Am. Chem. Soc. **119**, 5690 (1997).
[84]K. Kumar, I. V. Kurnikov, D. N. Beratan, D. H. Waldeck, and M. B. Zimmt, J. Phys. Chem. A **102**, 5529 (1998).
[85]S. Tsuneyuki, T. Kobori, K. Akagi, K. Sodeyama, K. Terakura, and H. Fukuyama, Chem. Phys. Lett. **476**, 104 (2009).

[86]A. A. Stuchebrukhov, Chem. Phys. Lett. **265**, 643 (1997).
[87]The coordinates of both the ala_{10}'s were taken from the Jena Library of Biological Macromolecules (JenaLib); see http://www.fli-leibniz.de/IMAGE.html.
[88]M. W. Schmidt, K. K. Baldridge, J. A. Boatz, S. T. Elbert, M. S. Gordon, J. H. Jensen, S. Koseki, N. Nasunaga, K. A. Nguyen, S. J. Su, T. L. Windus, M. Dupuis, and J. A. Montgomery, J. Comput. Chem. **14**, 1347 (1993).
[89]J. S. Binkley and J. A. Pople, J. Am. Chem. Soc. **102**, 939 (1980).
[90]W. J. Hehre, R. Ditchfield, and J. A. Pople, J. Chem. Phys. **56**, 2257 (1972).
[91]R. Krishnan, J. S. Binkley, R. Seeger, and J. A. Pople, J. Chem. Phys. **72**, 650 (1980).
[92]T. H. Dunning, J. Chem. Phys. **90**, 1007 (1989).
[93]M. J. Frich, J. A. Pople, and J. S. Binkley, J. Chem. Phys. **80**, 3265 (1984).
[94]See supplementary material at http://dx.doi.org/10.1063/1.3594100 for the canonical MO energy spectra obtained with the cc-pVDZ basis set in the TCNE-$(C_6H_6)_6$-TCNE system, dependence of T_{DA} on n in the TCNE-$(C_6H_6)_n$-TCNE systems calculated with the 3-21G basis set, and the Green function matrix elements obtained in both the ala_{10} systems with $E_{tun} = -1.0$ eV and $E_{tun} = -5.0$ eV.
[95]H. Tatewaki and S. Huzinaga, J. Comput. Chem. **1**, 205 (1980).
[96]M. A. Ratner, J. Phys. Chem. **94**, 4877 (1990).
[97]H. Umeda, Y. Inadomi, T. Watanabe, T. Yagi, T. Ishimoto, T. Ikegami, H. Tadano, T. Sakurai, and U. Nagashima, J. Comput. Chem. **31**, 2381 (2010).
[98]H. Nishioka and T. Kakitani, J. Phys. Chem. B **112**, 9948 (2008).